Chapter 10

Radiation losses and particle injection studies

10.1 Introduction

Empirical models of the radiation belts such as the ECM97 model developed in this study (see Chapter 9) are compilations of the data gathered over a period of time collected in bins of finite size. The coverage may not be complete, and the statistical errors in some bins may be greater than in others. There is a need therefore to have some means of smoothing, interpolating and perhaps extrapolating the data to improve the value and coverage of the model. While it is quite possible to use arbitrary functions such as polynomials, it is better to use functions which have an underlying relationship to the physics of the system. In Technical Note 8 we set out to find appropriate functions to fit to the pitch angle distributions measured by the MEA detector on CRRES. We took the averaged values of the flux over the pitch angle range covered by the instrument and relate them to the distributions which would result from the mechanism of pitch angle diffusion. It must be borne in mind that pitch angle diffusion could properly only be related to instantaneous observations of the complete distribution and it is questionable whether diffusion coefficients obtained from averaged distributions have any real significance.

Nevertheless the fitted distributions give a good idea of how the process of pitch angle diffusion varies throughout the outer electron radiation belts and how the loss rates of trapped electrons vary with L. The analysis has not been successful in deriving the flux within the loss cone and so the final loss rates could not be calculated but the results provide a better means of extrapolating the measurements of CRRES down to low altitudes than the previous technique which was used to extrapolate low altitude measurements to the equatorial region for input to the AE-8 model. In addition the results can be used to adjust the observations of the ISEE electron detectors for input to a directional intensity model of the radiation belts. The data in the current ISEE model were obtained from a set which contained omnidirectional energy spectra, and pitch angle distributions summed over all energies. It then had to be assumed that all energies had the same pitch angle distribution. The results here show that assumption to be inaccurate, and any distribution summed over the energy range will be dominated by the angular

distribution of the lowest energy, which is numerically greatest. The lowest energies are at one extreme of the range of behaviour of pitch angle diffusion encountered in the radiation belts and therefore low energy pitch angle distributions will give a misleading impression at the highest energies. For a complete intercomparison of the MEA and ISEE data sets it will be necessary to take these effects into consideration. A further value of obtaining a parametric fit to the data is that the complete data set can be summarized accurately with a much smaller set of numbers. A model could then be specified with a much smaller set of numbers.

10.2 Theoretical background

The main loss mechanism for radiation belt electrons is by precipitation into the atmosphere. Electrons in trapped orbits are scattered randomly in pitch angle by plasma waves and ultimately reach the loss cone by diffusion. The process is most likely to be self-driven; that is, the energy for the waves comes from the particles themselves because as they scatter towards smaller pitch angles they lose energy to wave growth. Alternatively the electrons may be scattered by externally generated waves. Whatever the source of waves the effect is the same; the particles diffuse in pitch angle towards the loss cone and as a result their distribution develops a maximum at 90° and decreases monotonically towards the field-aligned direction. The process has been analysed mathematically by a number of authors (Wentworth 1963, Walt & MacDonald 1964, Kennel & Petschek 1966, Roberts 1969, Schultz & Lanzerotti 1974) by deriving a diffusion equation from the Fokker-Planck equation. We followed the development of Roberts (1969).

If the source function is independent of time the solution of the Fokker-Planck equation can be written in the form:

$$j(\mu_0, t) = j_{\mathrm{s}}(\mu_0) + \sum_{n=1}^{\infty} a_n \, j_n(\mu_0) \, \mathrm{e}^{-\eta_n t}, \tag{10.1}$$

where $j_n(\mu_0)$ are the normal modes solutions, which can be defined in terms of Bessel functions of the first kind J_n (see Technical Note 8), and η_n are the decay constants. We are not interested in the steady state solution $j_{\mathrm{s}}(\mu_0)$ in which the source is balanced by the loss of particles to the atmosphere and so we ignore it and the source term itself.

If the initial distribution is complex in shape a number of terms in the expansion may be required to fit the profile. However, it can be shown that the higher order terms lead to larger values for the decay constant η and so they rapidly die away leaving the lowest order term to dominate. Thus for our solution we are left with the zero order Bessel function of the first kind in the following form:

$$j_1(\mu_0) = J_0 \left[\zeta_1 \left(\frac{\mu_0}{\mu_{\mathrm{c}0}} \right) \right] . \tag{10.2}$$

It has been assumed so far that the intensity at $\mu_0 = 0$, i.e. at a pitch angle of 90°, is normalized so that $j_1(0) = 1$. In fact, $J_0(x) = 1$ at $x = 0$. In order to be able to fit to the data we use the following form:

$$j(\mu_0) = j(0) \, J_0 \left(\frac{\mu_0}{\mu_{\mathrm{sc}}} \right) . \tag{10.3}$$

Thus we could fit the two parameters $j(0)$ and $\mu_{\rm sc}$ by the following procedure. $j(0)$ can be obtained from the intensity at 90° pitch angle and $\mu_{\rm sc}$ from the ratio of the flux at the edge of the loss cone to the intensity at 90° by solving the following equation for $\mu_{\rm sc}$:

$$\frac{j(\mu_{\rm c0})}{j(0)} = J_0\left(\frac{\mu_{\rm c0}}{\mu_{\rm sc}}\right) . \tag{10.4}$$

In fact, the procedure we shall use is to make a least squares fit to the data involving measurements at a number of pitch angles between 90° and the edge of the loss cone. Note also that our parameter $\mu_{\rm sc}$ is equivalent to Roberts' (1969) parameters as follows:

$$\mu_{\rm sc} = \frac{\mu_{\rm c0}}{\zeta_{\rm vn}} . \tag{10.5}$$

This solution meets the boundary condition that the slope of the function at 90° is zero and that it is therefore symmetric about 90°. This applies outside the loss cone; inside the loss cone a different solution is required to meet different boundary conditions. There we use the alternate Bessel function $I_0(x)$ which has the properties that it is equal to 1 at $x = 0$, and increases monotonically as x increases. In this case the function is:

$$j(\alpha_0) = j(\alpha = 0)\, I_0\left(\frac{\alpha_0}{\alpha_{\rm sc}}\right) . \tag{10.6}$$

We use the intensity at the edge of the loss cone obtained from the Bessel function fit described above and the measured intensity at a pitch angle of 2.5°, which is the minimum pitch angle available. The ratio of the two quantities gives $\alpha_{\rm sc}$ by solving:

$$\frac{j(\alpha = 2.5^\circ)}{j(\alpha_{\rm c0})} = \frac{I_0\left(\frac{\alpha = 2.5^\circ}{\alpha_{\rm sc}}\right)}{I_0\left(\frac{\alpha_{\rm c0}}{\alpha_{\rm sc}}\right)} . \tag{10.7}$$

The value of $j(\alpha = 0)$ is found by matching the two functions at the edge of the loss cone.

10.3 Relation to the work of Vampola (1996)

Vampola (1996) used the CRRES/MEA data and magnetic activity as the input to a neural network which could then be used to estimate the radiation belt intensities over a much wider period of time than the duration of the CRRES mission. He made fits to the pitch angle distribution in order to be able to extrapolate the measurements of CRRES/MEA from a position off the equator to the equatorial plane. The function he used was $\sin^n \alpha$, where the exponent n was obtained from the ratio of the flux at 90° to the flux at 45°. The reason he used the function apart from its simplicity was that the functional form remains the same as one moves along the field line. Figure 10.1 compares the sine function form with the equivalent Bessel function form for a value of n in the middle of the range of values found by Vampola, i.e. $n = 2$. The value of

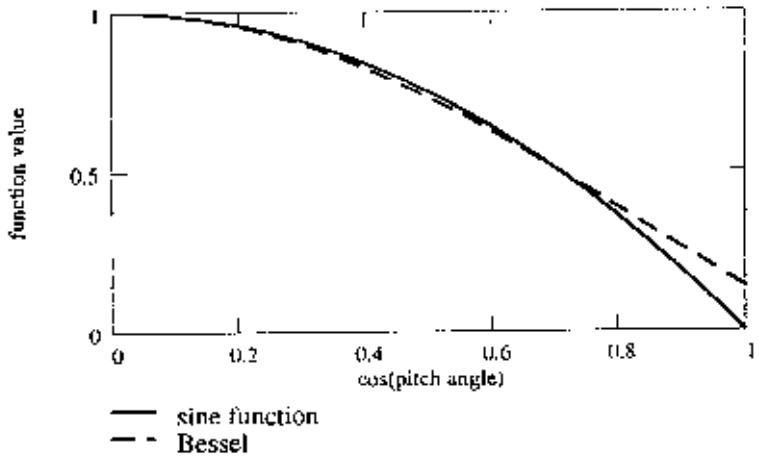

Figure 10.1. A comparison between a Bessel function and a sine function fitted between the same two points, at 90° and at 45°

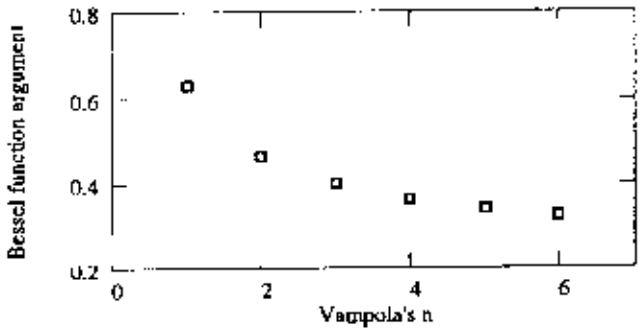

Figure 10.2. The relation between the parameter n from Vampola's (1996) fits and the Bessel function fit from this work

$\mu_{\rm sc} = 0.465$ has been obtained by ensuring that both give the same value at 45°. The diagram shows that the two functions are very similar from $\mu_0 = \cos\alpha = 0$ to $\mu_0 = 0.8$ where the pitch angle is 37°. There is a very crucial difference near the loss cone where the sine function goes to zero at a pitch angle of zero. This is not the physical reality since the intensity at zero pitch angle in general has a finite value. Thus the sine function is not useful for studying what happens in or near the loss cone. Figure 10.2 compares the range of values of n obtained by Vampola with the equivalent values of $\mu_{\rm sc}$. These values lie in the range found by the analysis reported here, and the radial variation is approximately equivalent. Thus these results and those of Vampola are consistent with each other.

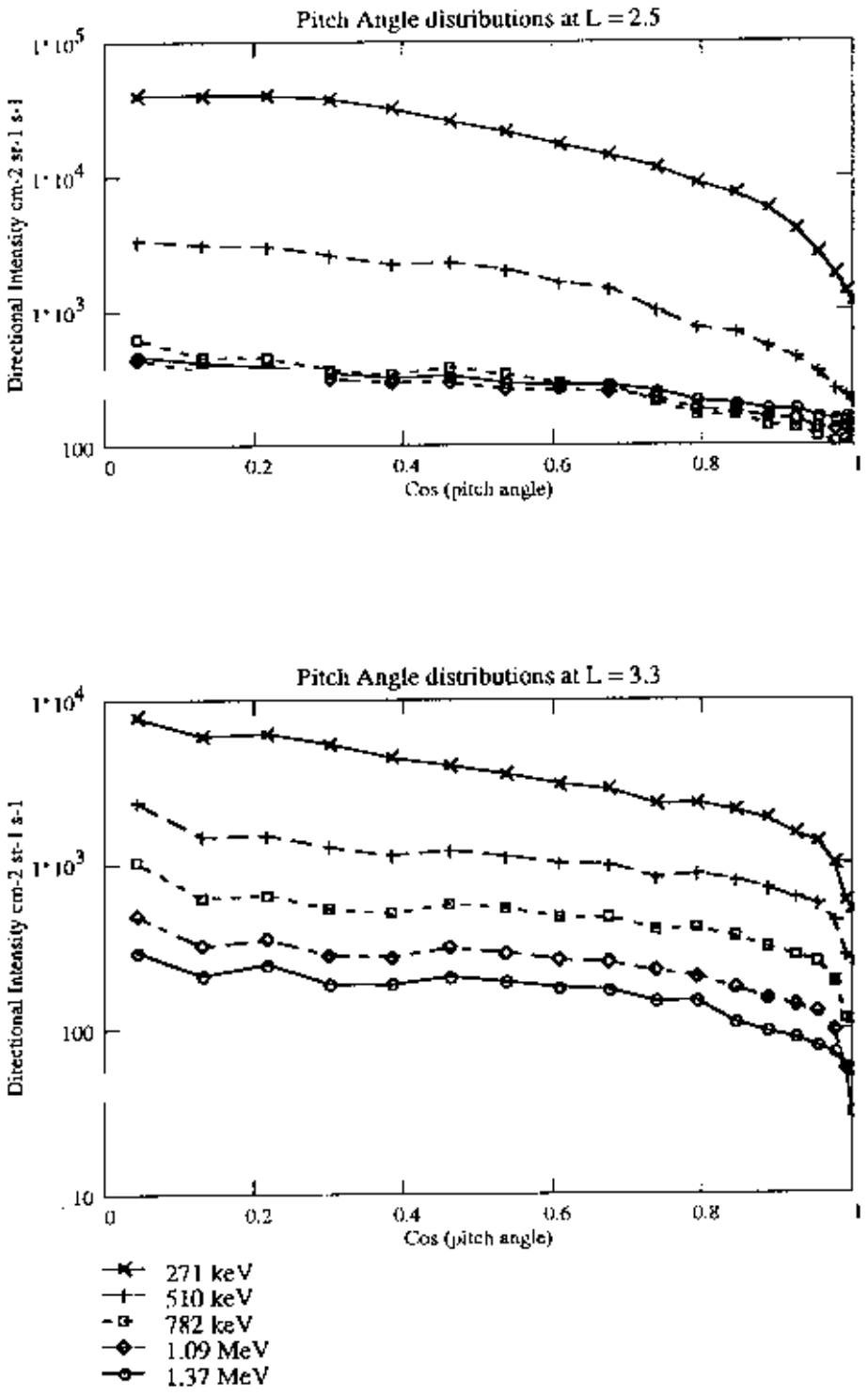

Figure 10.3. Pitch angle distributions for $K_{\rm p} = 0$ to 1^+, for $L = 2.5$ and $L = 3.3$

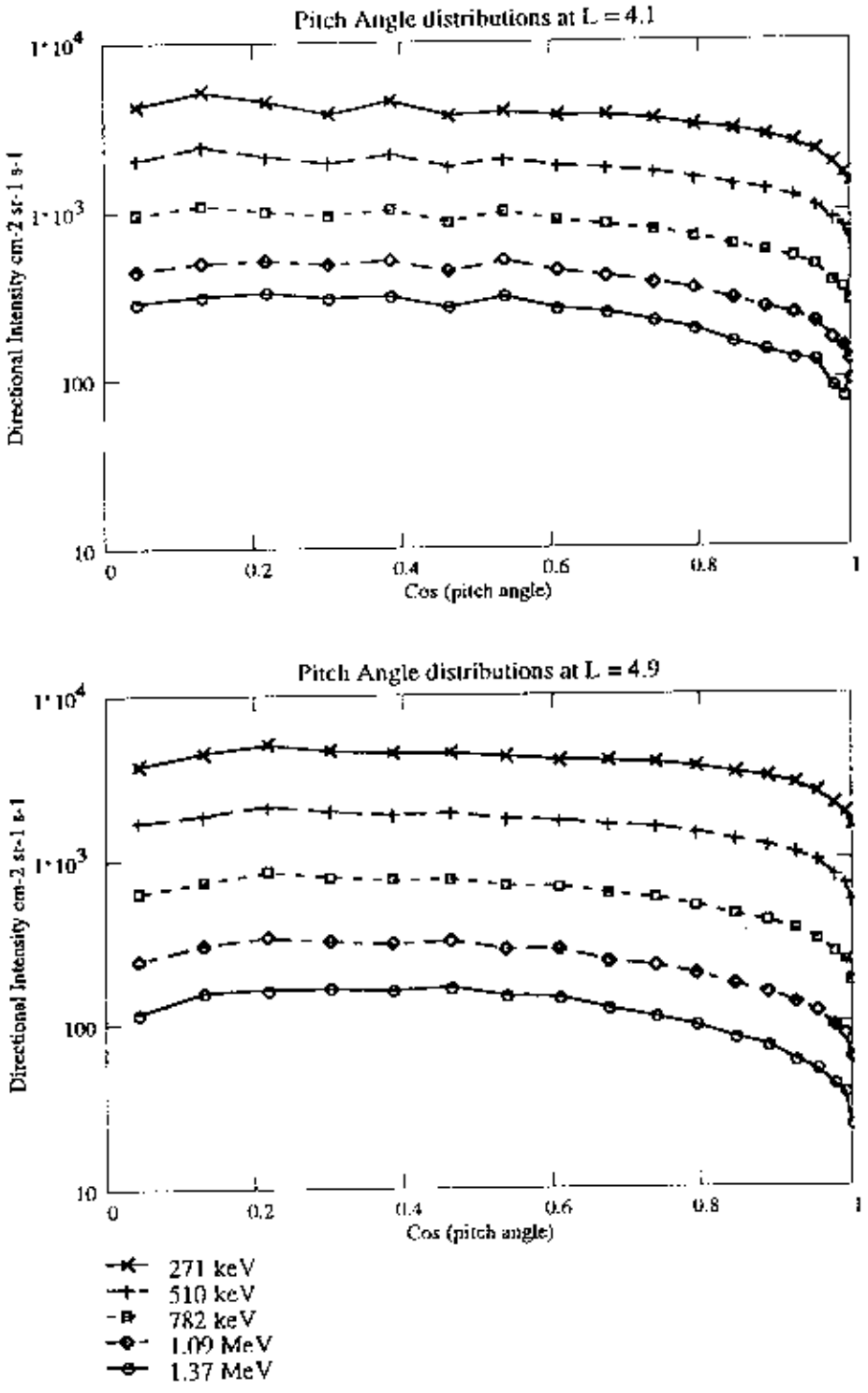

Figure 10.4. Pitch angle distributions for $K_{\mathrm{p}} = 0$ to 1^{+}, for $L = 4.1$ and $L = 4.9$

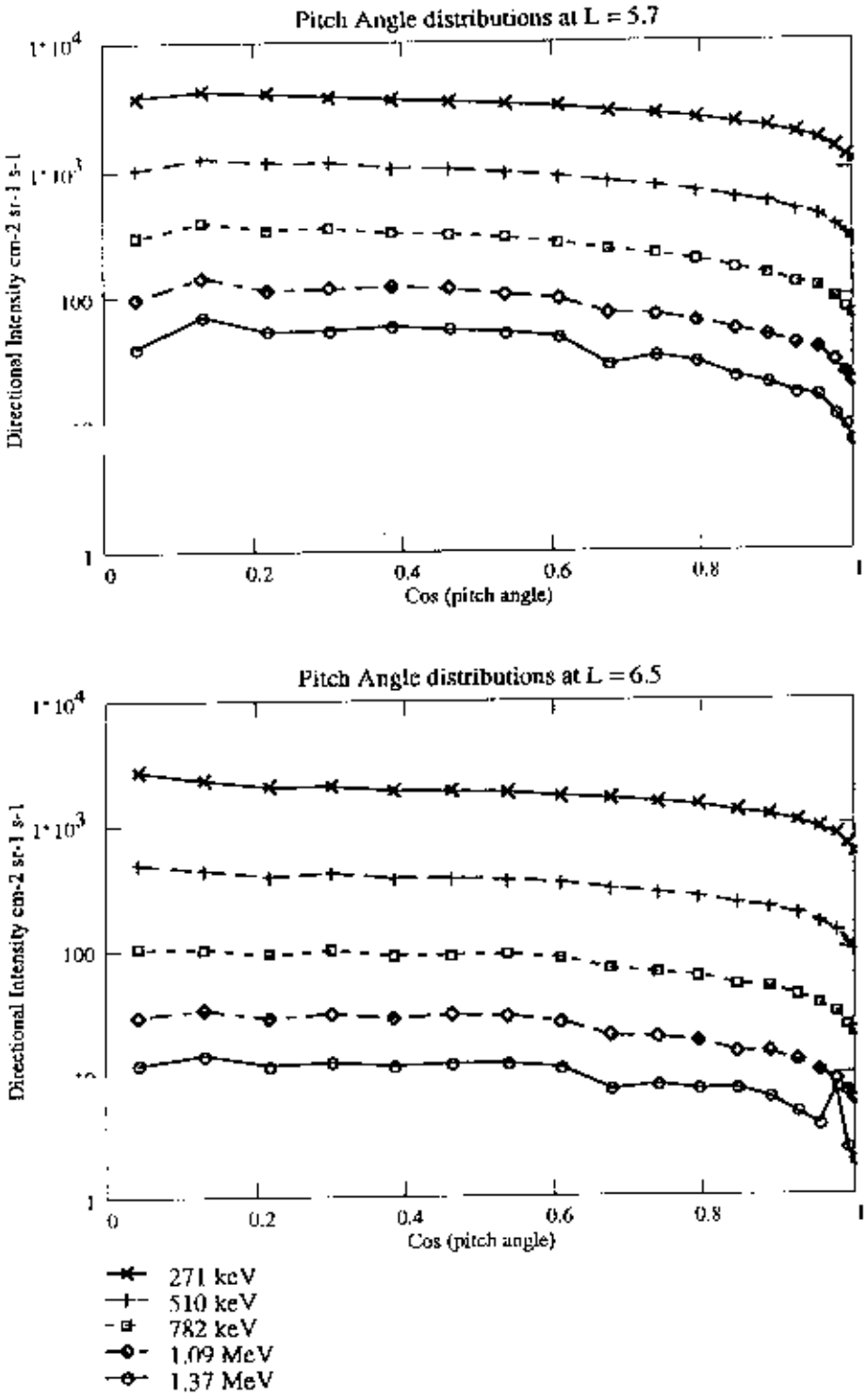

Figure 10.5. Pitch angle distributions for $K_{\rm p} = 0$ to 1^+, for $L = 5.7$ and $L = 6.5$

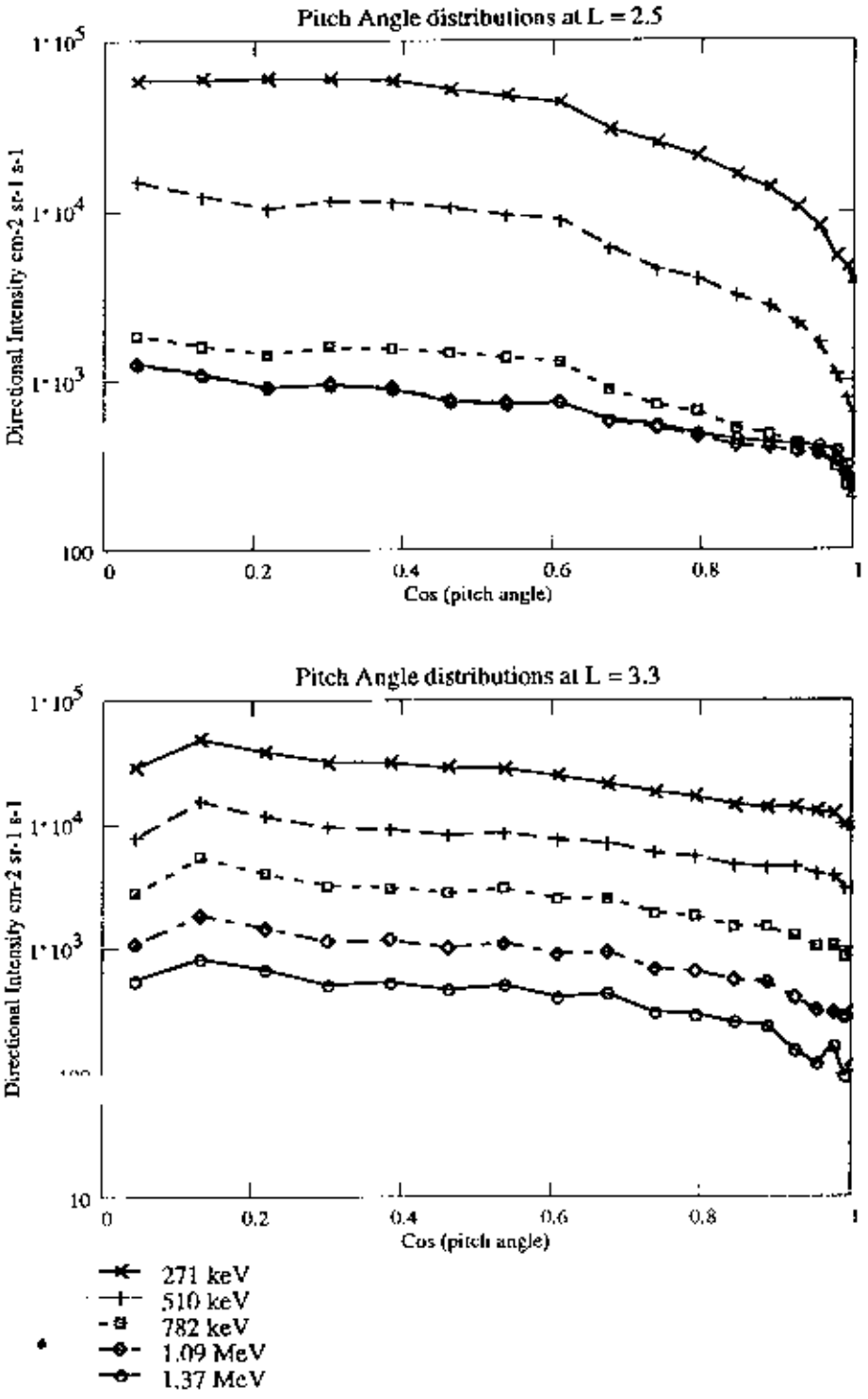

Figure 10.6. Pitch angle distributions for $K_{\mathrm{p}} = 6$ to 7^{+}, for $L = 2.5$ and $L = 3.3$

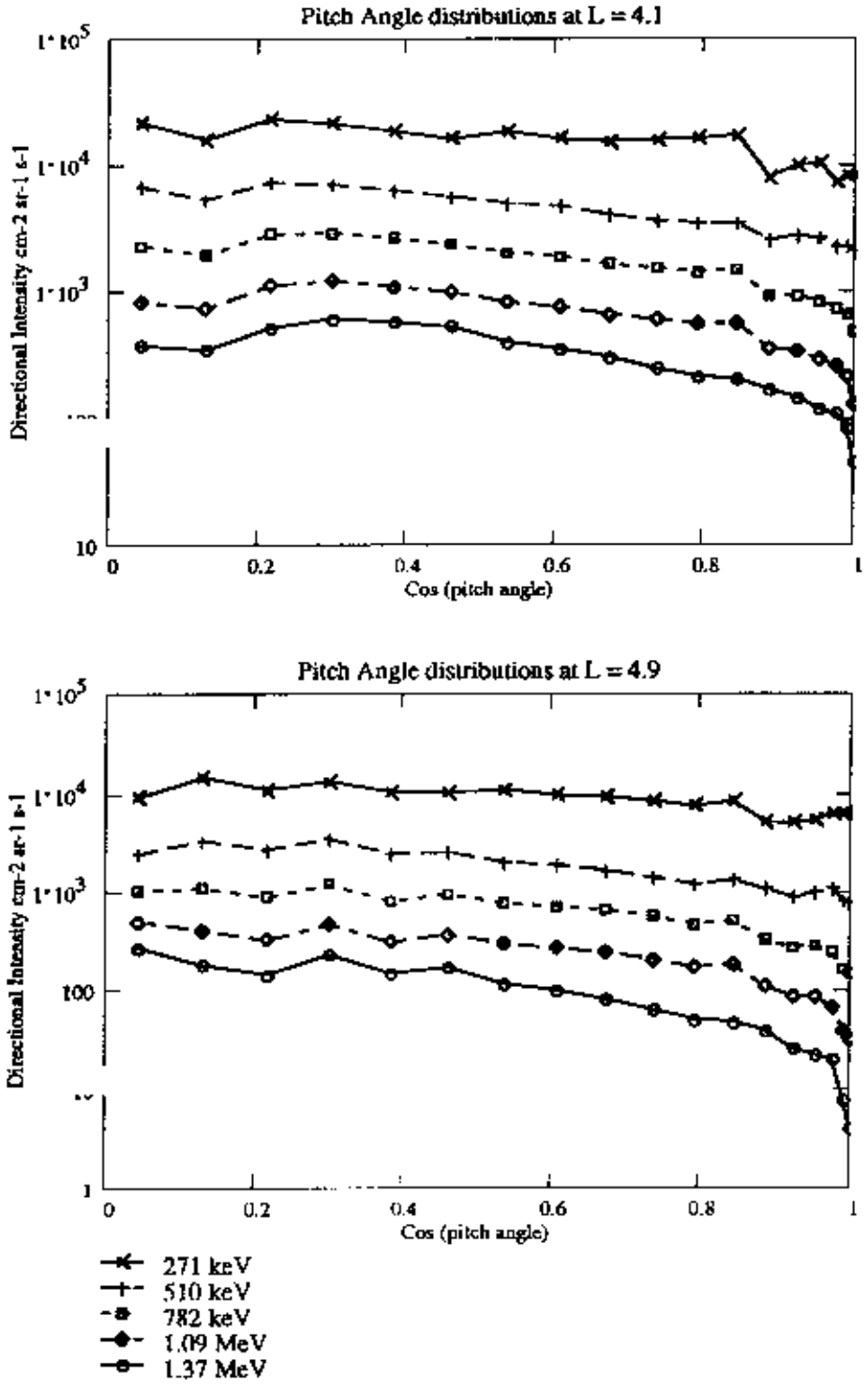

Figure 10.7. Pitch angle distributions for $K_{\rm p} = 6$ to 7^+, for $L = 4.1$ and $L = 4.9$

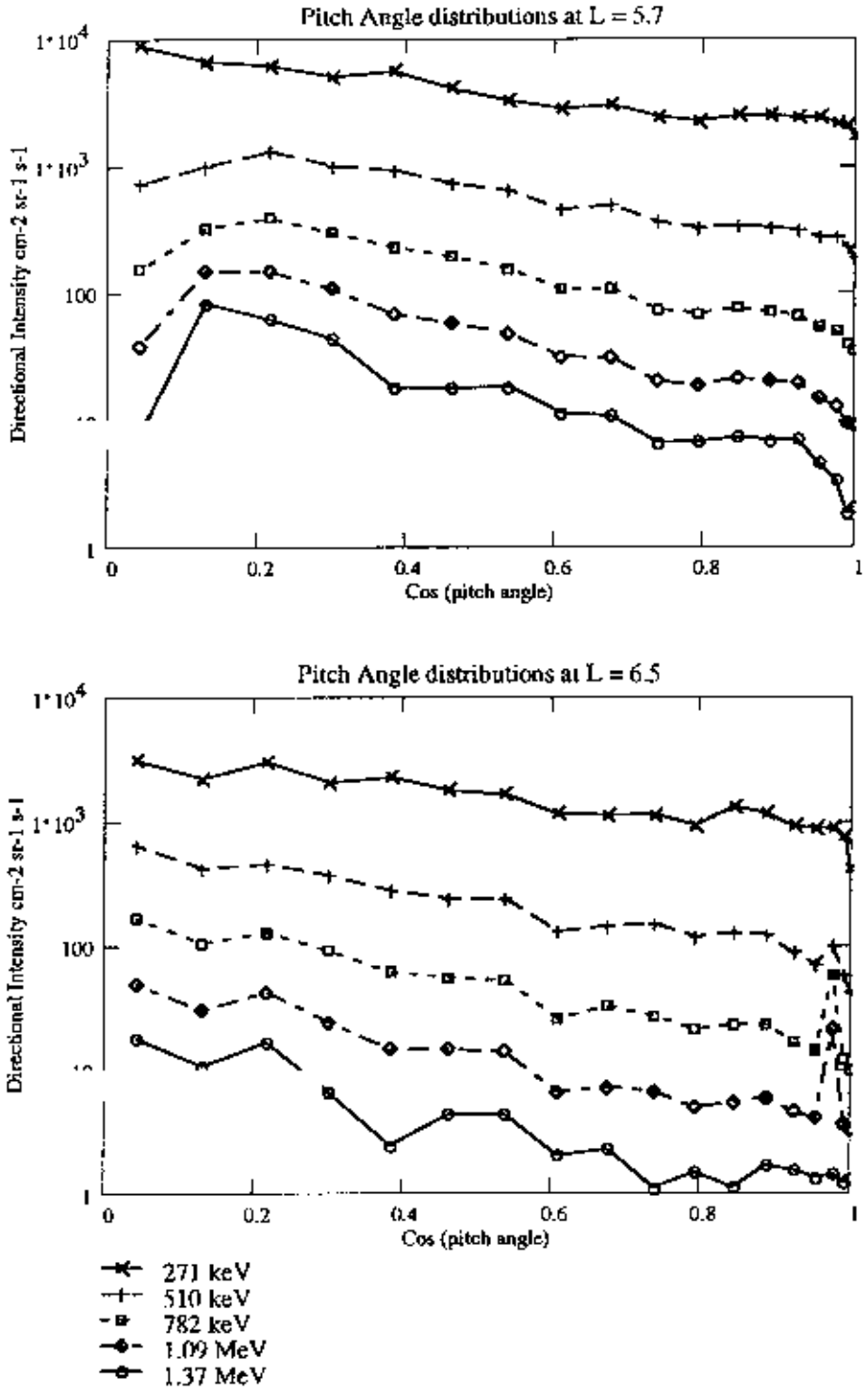

Figure 10.8. Pitch angle distributions for $K_{\mathrm{p}} = 6$ to 7^{+}, for $L = 5.7$ and $L = 6.5$

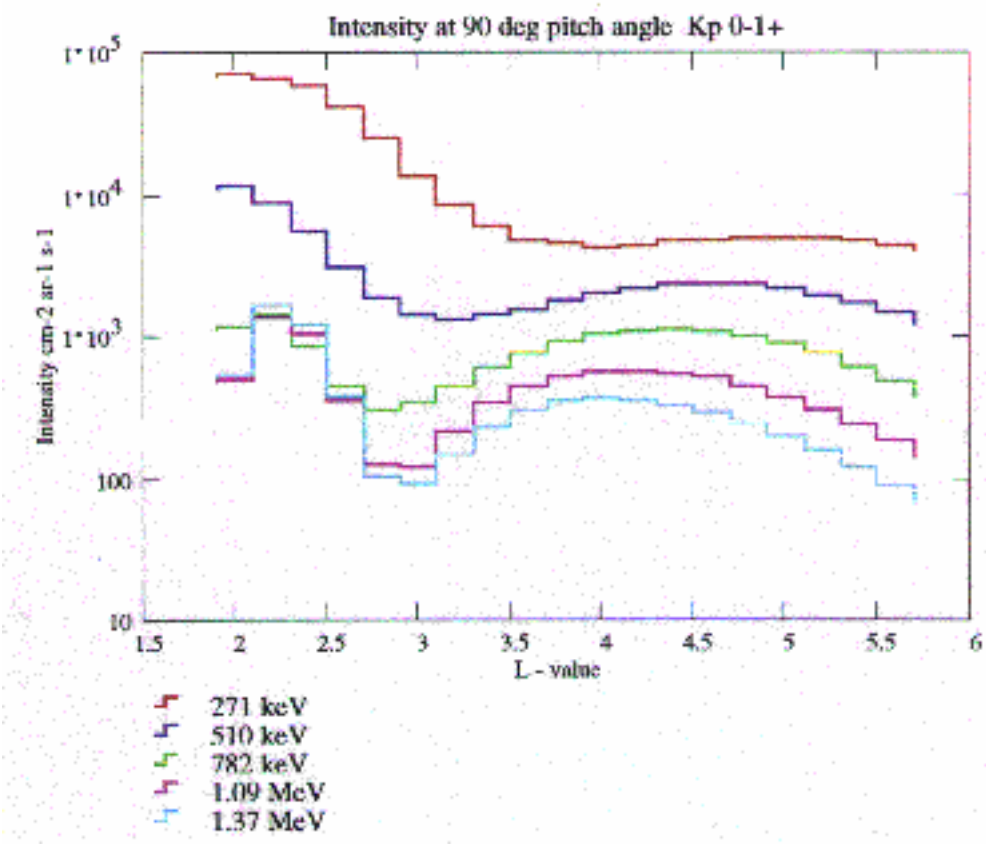

Figure 10.9. The electron intensity at 90° pitch angle obtained by fitting a Bessel function to the complete distribution as a function of L, for low K_{p} values. Note that at the highest energies and the lowest L values the overlapping curves indicate that the measurements are contaminated by penetrating protons.

10.4 Pitch angle distributions in the outer electron belt

The first step is to examine the shape of the angular distributions in the ECM97 model for a selection of energies at a selection of L values to establish the normal behaviour. The selected energies are distributed evenly through the range covered by MEA, namely 271 keV, 510 keV, 782 keV, 1.09 MeV, and 1.37 MeV, and the L values are 2.5, 3.3, 4.1, 4.9, 5.7, and 6.5. The distributions shown in Figs. 10.3–10.5 are for K_{p} at the lowest level, of 0 to 1^{+}. The distributions in Figs. 10.6–10.8 are at the high level of $K_{\mathrm{p}} = 6$ to 7^{+}. Some of the points to notice are:

1. the intensity decreases with energy at all distances;
2. the minimum intensity is always at a pitch angle of zero;
3. there are examples of a local minimum at 90°, mainly at high energies and large distances;
4. the distributions tend to be more anisotropic at the higher energies;
5. the distributions tend to be more anisotropic at lower altitudes;

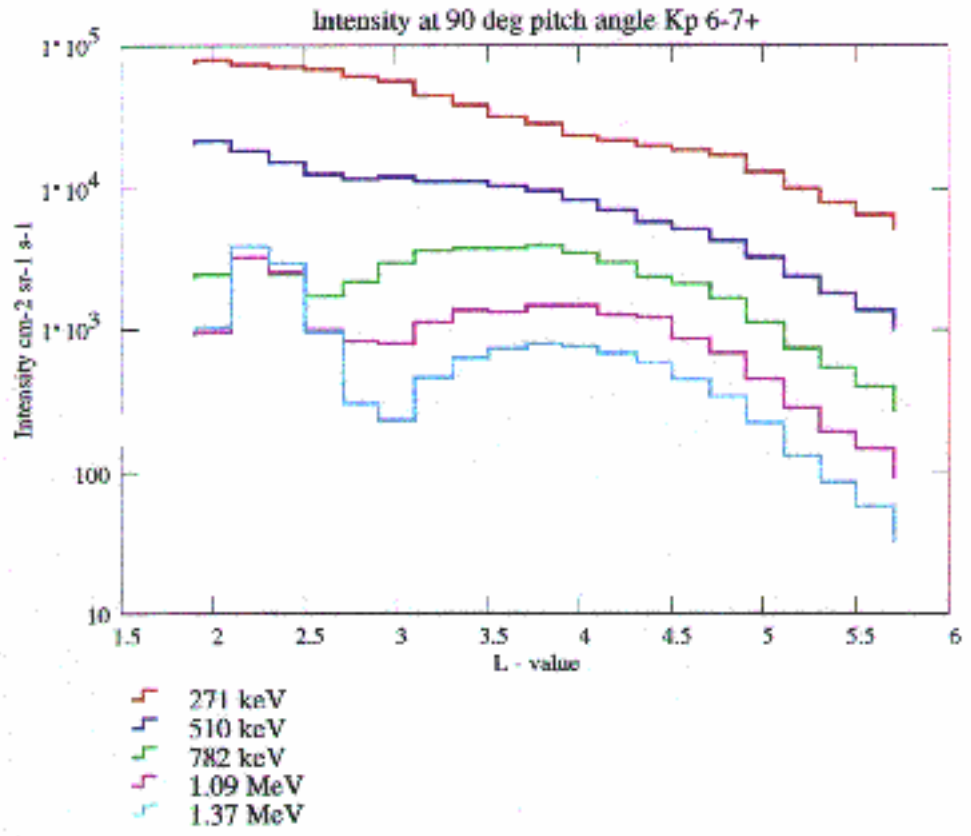

Figure 10.10. The electron intensity at 90° pitch angle obtained by fitting a Bessel function to the complete distribution as a function of L, for high K_{p} values

6. the minimum in the loss cone tends to be deeper at higher energies;
7. the variation between energies and/or distance is smooth and apparently continuous;
8. while there is some statistical scatter there is not enough to make fitting difficult;
9. at $L = 2.5$ there is a detectable background from penetrating protons which render the measurements at the two highest energies, where the intensity is smallest, inaccurate and unusable.

Except for point 1 the similarity to the Bessel function variation is close. The minimum at 90° cannot be generated by pitch angle diffusion and from the magnitude of the scatter over the rest of the pitch angle range and the consistency of the minimum from one distribution to nearby ones it cannot be the result of statistical variation. In fact such pitch angle distributions are well-known, and usually called “butterfly” distributions. The explanation for them is “shell splitting” whereby particles at different pitch angles follow different drift shells. They are most noticeable where there is a steep negative spatial gradient in intensity so that the small difference in drift shell has a large effect on intensity. In deriving the Bessel function fit, pitch angles near 90° have

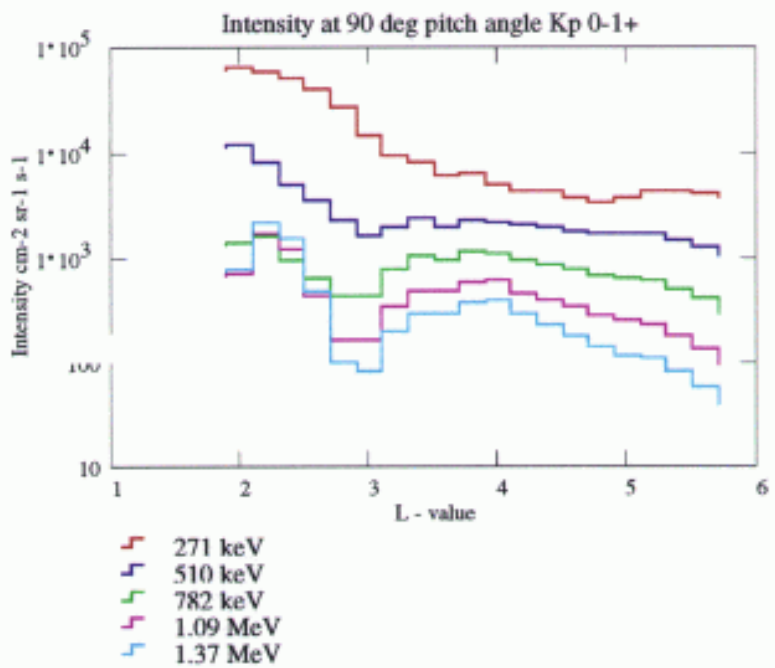

Figure 10.11. The electron intensity at 90° pitch angle measured by the CRRES/MEA detector, as a function of L, for low K_{p} values. Note that at the highest energies and the lowest L values the overlapping curves indicate that the measurements are contaminated by penetrating protons.

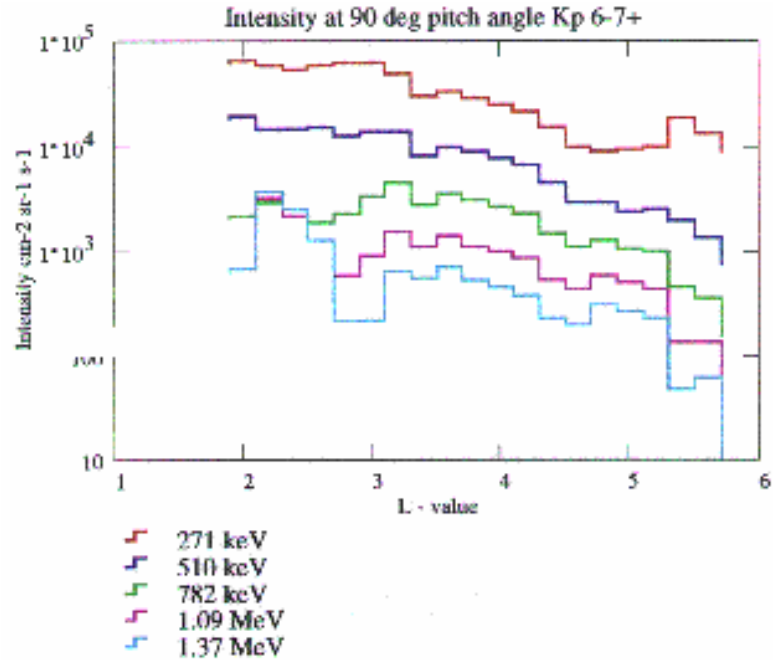

Figure 10.12. The electron intensity at 90° pitch angle measured by the CRRES/MEA detector, as a function of L, for high K_{p} values

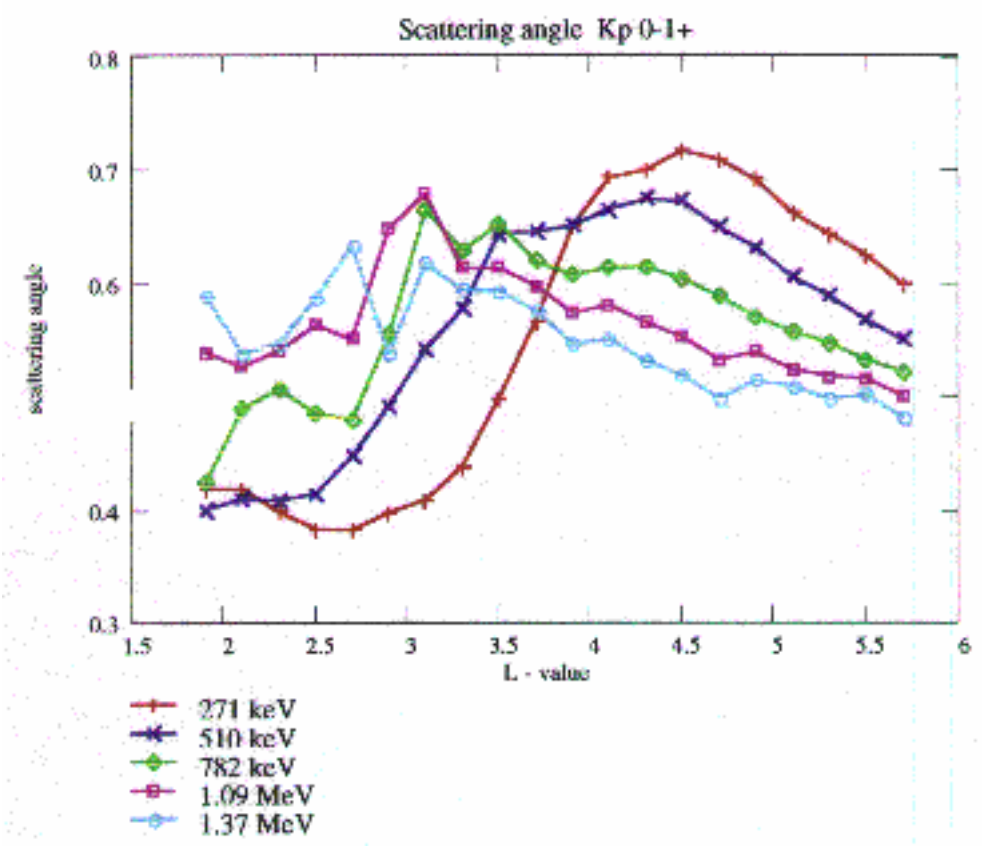

Figure 10.13. The scattering angle derived from the Bessel function fit at five energies over the entire L range for low K_{p} values. Note that the measurements inside $L = 2.7$ and at the three highest energies are contaminated by penetrating protons.

been excluded, as have pitch angles in or close to the loss cone in order to avoid the influence of these effects. The fit is based on the intermediate angles. The shell-splitting minimum did upset Vampola's fit of the sine function since he based it always on the ratio of the intensities at 90° to that at 45°. He records that when the intensity at 45° was the greater he excluded the data.

10.5 Fitting a Bessel function to the distribution outside the loss cone

The mathematical basis for the fitting process is described in Sect. 10.2. The software used was the Mathcad Plus package for Macintosh. The nature of the software is such that it is not possible to carry out the fit for more than one energy at a time. It is done at each L value in the ECM97 model, i.e. at intervals of 0.2 in L, and for the same two K_{p} levels as before. The results from successive runs at the same sequence of energies as used in the pitch angle plots

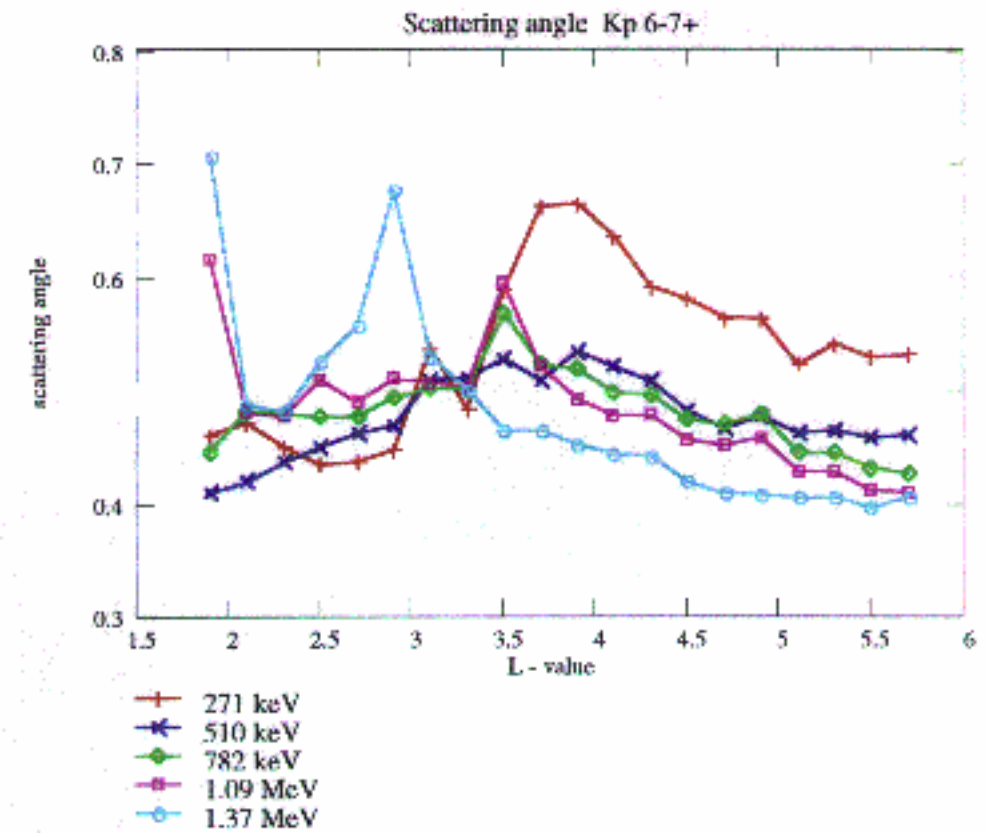

Figure 10.14. The scattering angle derived from the Bessel function fit at five energies over the entire L range for high $K_{\rm p}$ values. Note that the measurements inside $L = 2.7$ and at the three highest energies are contaminated by penetrating protons.

were combined together for plotting and the results are shown in Figs. 10.9–10.14. Figures 10.9 and 10.10 show the radial variation of the equatorial intensity, which is obtained from the parameter $j(0)$ defined in Eq. (10.3) and which, of course, ignores the minimum arising from the butterfly distributions. Figure 10.9 shows the variation for the weakest $K_{\rm p}$ values of 0 to 1^+ and Fig. 10.10 for 6 to 7^+. The interesting feature about the comparison is that the intensities at $L < 3$ and at $L > 5.5$ are very similar for the two $K_{\rm p}$ values. The biggest differences are in the L range from 3.5 to 4.5 and at the lowest energy. It is also apparent that the fitting process fulfils one of its functions outlined in the introduction—it smooths the data from the model. Figures 10.11 and 10.12 show the corresponding data based on just the intensity at 90° from the ECM97 model where there is clear statistical variation which is removed by the fitting process.

The next figures, Figs. 10.13 and 10.14, show the variation of the parameter $\mu_{\rm sc}$ from Eq. (10.3). Figure 10.13 is derived from the low $K_{\rm p}$ model and shows clear systematic structure. A smaller value for $\mu_{\rm sc}$ indicates greater anisotropy. We note:

1. all curves show least anisotropy in the L range where the intensity peaks but the peak for the higher energies is found at smaller L values;

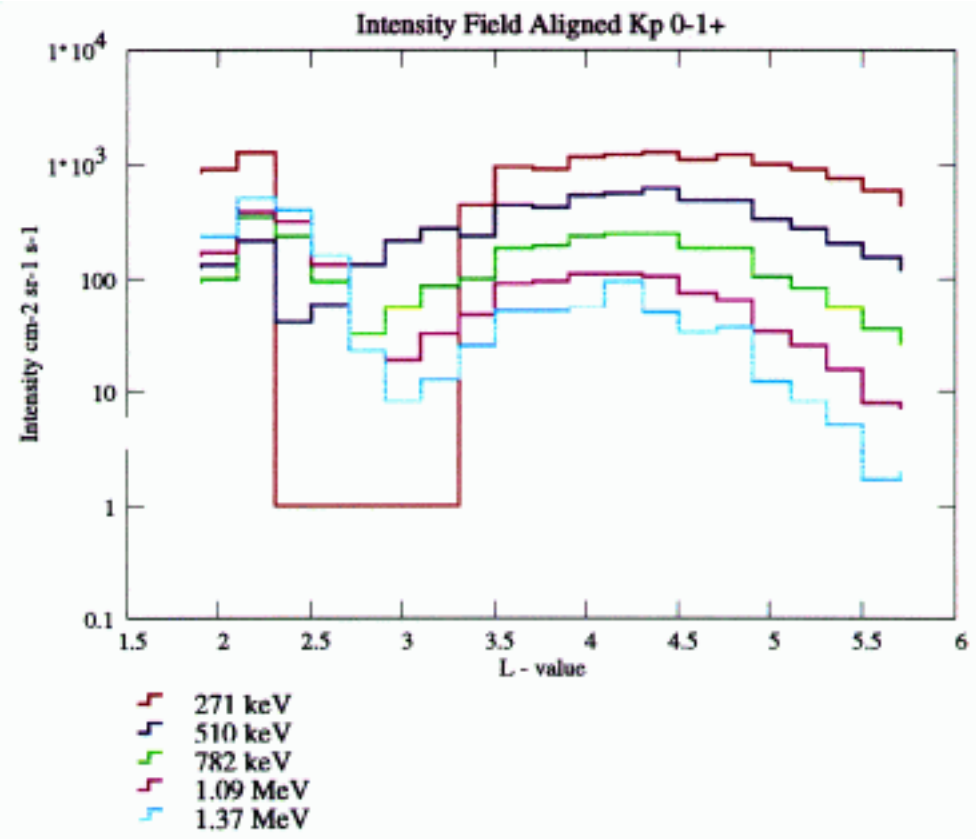

Figure 10.15. The intensity in the field aligned direction obtained from the Bessel function fit inside the loss cone at five energies over the entire L range for low $K_{\rm p}$ values. Note that the measurements inside $L = 2.7$ and at the three highest energies are contaminated by penetrating protons.

2. at large L values the lower energies have the largest $\mu_{\rm sc}$ value while at small L values the reverse is true.

In Fig. 10.14 the same features are visible but less clearly and the radial distance at which the changeover in behaviour occurs has moved closer to the Earth. The peak in $\mu_{\rm sc}$ is found near the peak intensity at the corresponding energy, and the peak intensities are also found at smaller L for higher energy but the relationship is not exact. Another relationship which should be explored is with the position of the plasmapause. The average position of the plasmapause is in the range $4.1 < L < 4.5$ but is further out and less sharp for lower $K_{\rm p}$.

10.6 Fitting a Bessel function to the distribution inside the loss cone

Two parameters are derived from the fit inside the loss cone: the intensity at zero pitch angle, or the field aligned intensity, and the second scattering angle $\alpha_{\rm sc}$. The field aligned intensity is the

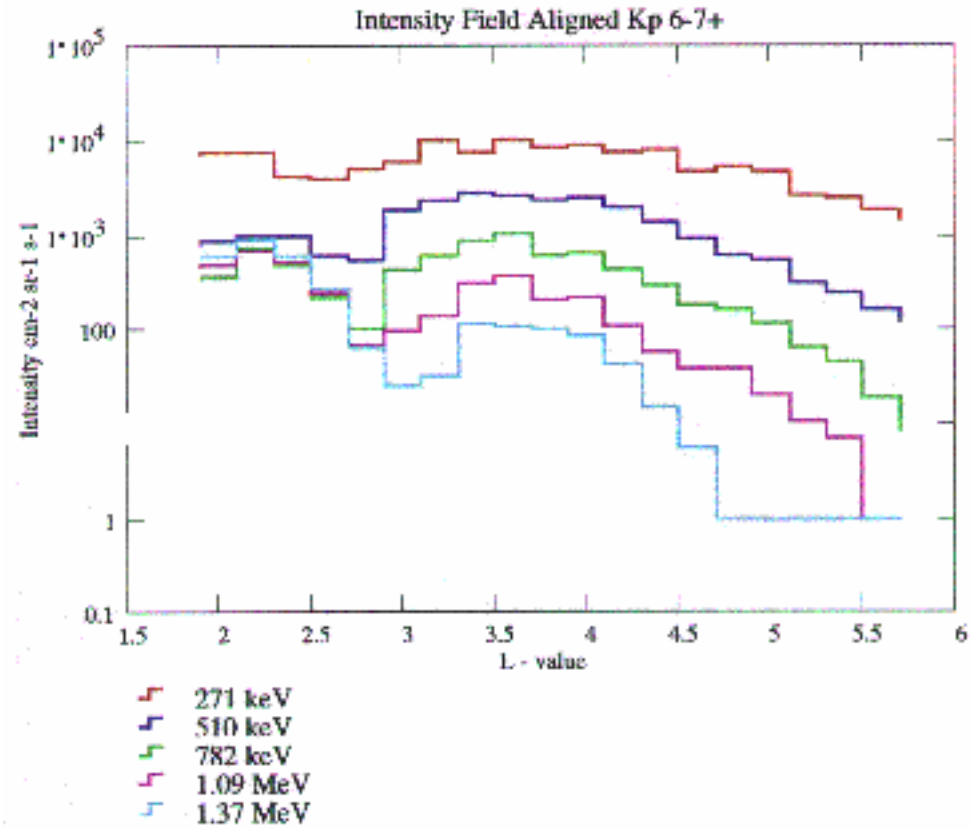

Figure 10.16. The intensity in the field aligned direction obtained from the Bessel function fit inside the loss cone at five energies over the entire L range for high $K_{\rm p}$ values. Note that the measurements inside $L = 2.7$ and at the three highest energies are contaminated by penetrating protons.

best measure of the loss rate as it corresponds directly to the numbers of particles being lost per second. Figures 10.15 and 10.16 show the field aligned intensity for the same set of energies and $K_{\rm p}$ values as usual. The features are:

1. there is a peak intensity but it is at the same radial distance for all energies in contrast to the 90° intensity;
2. the peak is in the range $4.1 < L < 4.5$ for $K_{\rm p}$ small and $3.3 < L < 3.7$ for $K_{\rm p}$ large, i.e. it is clearly inside the plasmapause in both cases;
3. the precipitating flux is smaller by a factor of approximately 5 in the low $K_{\rm p}$ case over the whole range again in contrast to the 90° intensity, i.e. as would be expected the precipitation rate is smaller for small $K_{\rm p}$.

The values of the scattering angle in the loss cone, $\alpha_{\rm sc}$, were the most difficult to obtain because the fitted intensity at the edge of the loss cone was often smaller than the measured value at a pitch angle of 2.5°. Also, outside $L = 5$, the edge of the loss cone is inside 2.5°. The results are

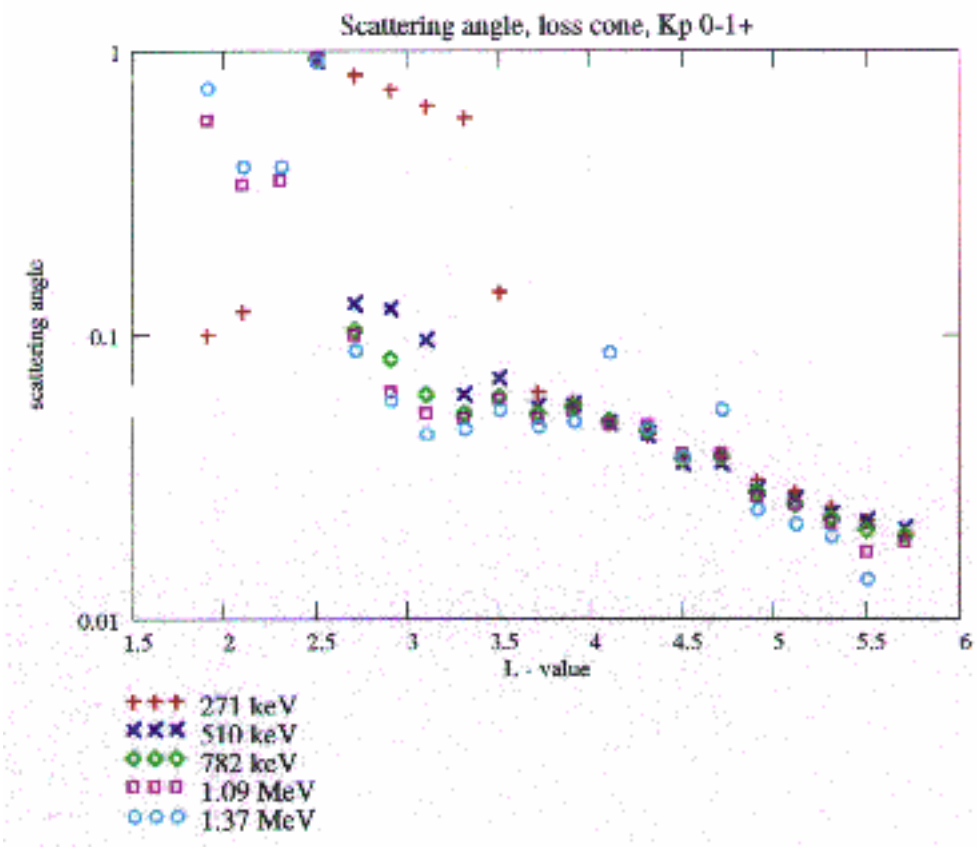

Figure 10.17. The scattering angle inside the loss cone obtained from the Bessel function fit at five energies over the entire L range for low $K_{\rm p}$ values. Note that the measurements inside $L = 2.7$ and at the three highest energies are contaminated by penetrating protons.

shown in Figs. 10.17 and 10.18 for the usual energies and $K_{\rm p}$ values. There is a wide scatter on the values in both plots. Referring first to Fig. 10.18 there is a nearly continuous line of points extending from 1 at $L = 2.5$ down to 0.2 at $L = 5.5$. These are the points where no curve could be fitted. A dummy value was put in the results and so these points should be ignored. In Fig. 10.17, there are only a few dummy points for $L < 3.5$. There is less scatter in Fig. 10.17 with a solid line of points from 0.1 at $L = 2.5$ to 0.02 at $L = 5.5$, with all energies nearly superimposed on each other. A careful inspection of the distribution of points reveals that in both cases there is a minimum at $L \sim 3$ and a maximum a little further out. This shape is consistent in all the curves. The magnitude of $\alpha_{\rm sc}$ is slightly smaller for low $K_{\rm p}$ and the minimum and maximum for low $K_{\rm p}$ are both slightly further out. In order to use the results for calculations of the loss rate it is necessary to remove the scatter. Since the variation through the maximum and minimum is relatively small a straight line has been fitted to the points on the log scale.

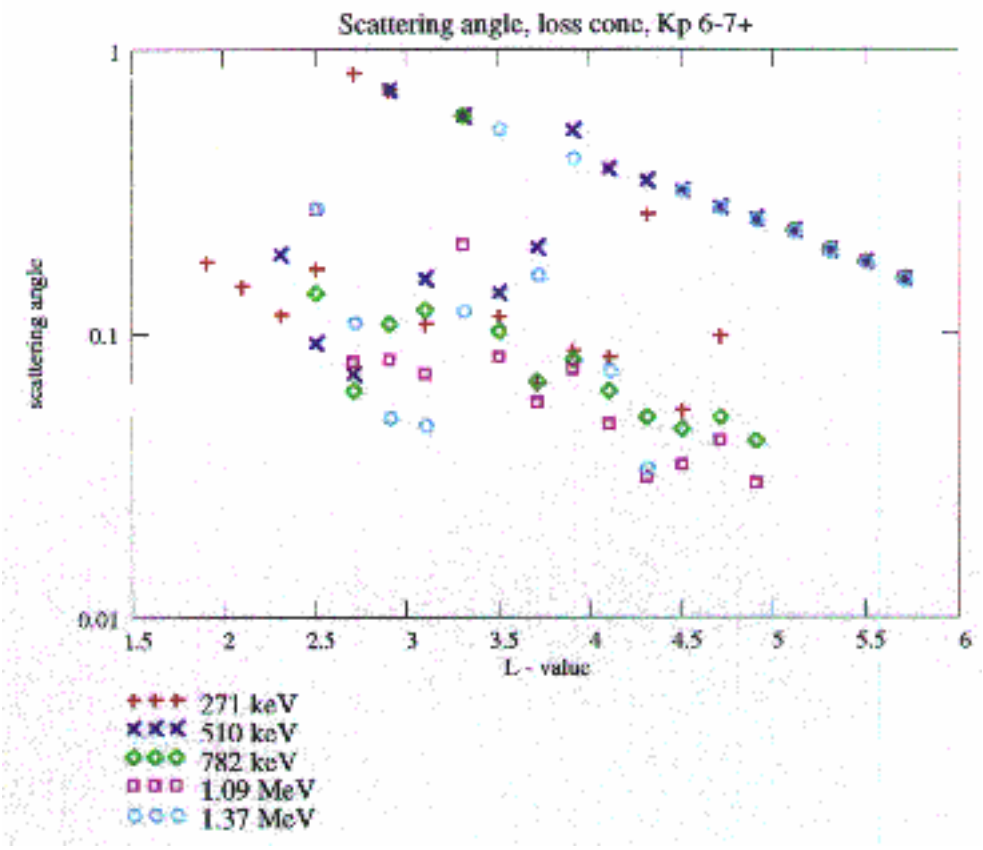

Figure 10.18. The scattering angle inside the loss cone obtained from the Bessel function fit at five energies over the entire L range for high $K_{\rm p}$ values. Note that the measurements inside $L = 2.7$ and at the three highest energies are contaminated by penetrating protons.

10.7 Estimated loss rates

If we know the distribution of particles from 90° to the field aligned direction then in principle the loss rate of the particles and the decay time of the radiation can be calculated.

The results of the calculation for the two $K_{\rm p}$ ranges are shown in Figs. 10.19 and 10.20. The values range from 10 seconds to 1000 seconds, with the smallest values for the lowest $K_{\rm p}$ range and smaller L values. These values are simply not realistic and do not accord with direct measurements of the decay times, which are normally in the range of 5 to 10 days (McIlwain 1996). Furthermore the times tend to be longer at smaller L values. The variation in Figs. 10.19 and 10.20 is dominated by the variation in the volume of the flux tube. Why, therefore, are the results clearly in error? The probable reason is that the flux in the loss cone is overestimated by the measurements of the MEA detector because a) the angular resolution is inadequate to resolve the loss cone over most of the L range, and b) there is probably some background noise which has its greatest effect where the count rates are at a minimum.

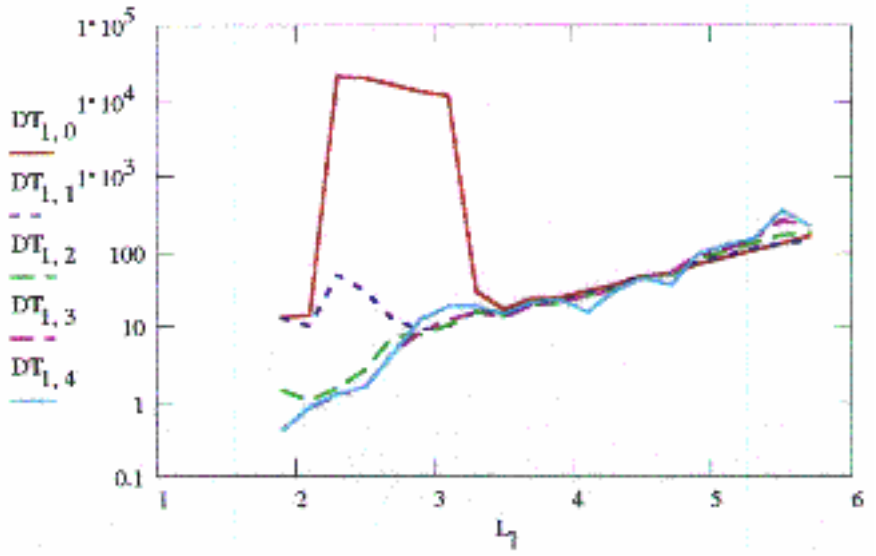

Figure 10.19. The decay time calculated for low K_{p} values. The peak at low L for 271 keV is an artifact due to missing data.

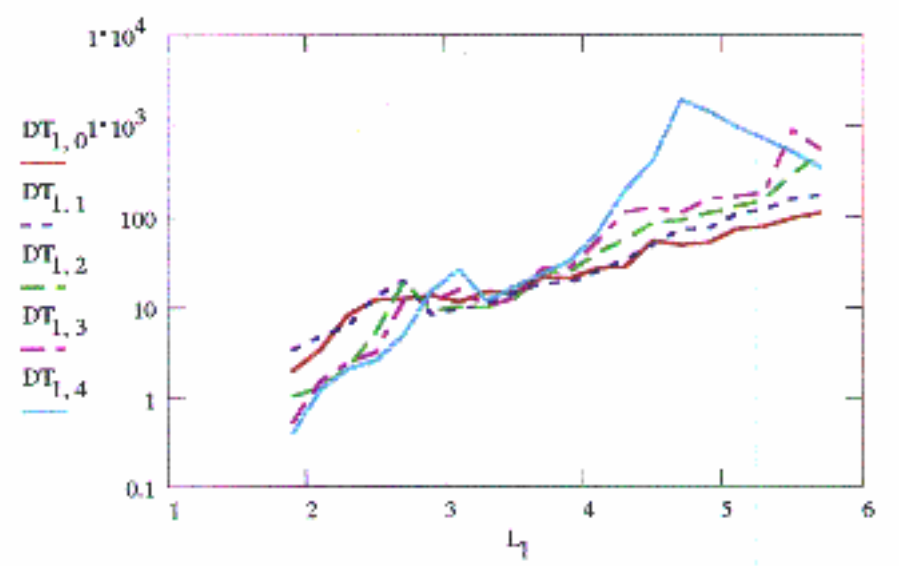

Figure 10.20. The decay time calculated for high K_{p} values

10.8 Conclusions

The use of the Bessel function to parameterise the pitch angle distribution works well in organizing and smoothing the data from the CRRES/MEA detector for pitch angles outside the loss cone. It shows that a model could be based on two parameters for the pitch angle distribution at each energy. One important feature which is not modelled is the existence of butterfly distributions. The effect on the average radiation intensity has not been evaluated but is not likely to be very important.

The two parameters $\mu_{\rm sc}$ and $j(0)$ vary systematically, and continuously, with L, energy and $K_{\rm p}$. Although it has not been done here, the parameters' dependence on these variables could be fitted with simple polynomial functions, thereby reducing the ECM97 model to analytical functions specified by, probably, less than 50 values instead of the current total of 61200 discrete values.

The MEA data is not adequate to specify the flux in the loss cone which is required to determine loss rates and to estimate the omnidirectional radiation levels at low altitudes. As an estimate of the lowest altitude at which the current model is reasonably accurate we take the altitude at which the loss cone is 20°.

The AE-8 model was based on data mainly obtained at low altitudes, and at geosynchronous orbit. Neither gives a good base for a complete model since, as the analysis here shows, only a small fraction of the distribution is actually measured (Vette 1991a).